nature nanotechnology

LETTERS

PUBLISHED ONLINE: 30 JANUARY 2011 | DOI: 10.1038/NNANO.2010.280

Time-dependent, protein-directed growth of gold nanoparticles within a single crystal of lysozyme

Hui Wei[1], Zidong Wang[2], Jiong Zhang[2], Stephen House[2], Yi-Gui Gao[3], Limin Yang[1,4], Howard Robinson[5], Li Huey Tan[1], Hang Xing[1], Changjun Hou[4], Ian M. Robertson[2]*, Jian-Min Zuo[2]* and Yi Lu[1,2]*

Gold nanoparticles are useful in biomedical applications due to their distinct optical properties and high chemical stability[1–5]. Reports of the biogenic formation of gold colloids from gold complexes has also led to an increased level of interest in the biomineralization of gold[6–13]. However, the mechanism responsible for biomolecule-directed gold nanoparticle formation remains unclear due to the lack of structural information about biological systems and the fast kinetics of biomimetic chemical systems in solution. Here we show that intact single crystals of lysozyme can be used to study the time-dependent, protein-directed growth of gold nanoparticles. The protein crystals slow down the growth of the gold nanoparticles, allowing detailed kinetic studies to be carried out, and permit a three-dimensional structural characterization that would be difficult to achieve in solution. Furthermore, we show that additional chemical species can be used to fine-tune the growth rate of the gold nanoparticles.

Among the many biological components that could participate in biomineralization and be incorporated into bio-nanomaterials, proteins have been the subject of particular attention due to their nanoscale dimensions, their various and distinctive molecular structures and functionalities, and their specificities and versatility in recognition and assembly. To date, most studies have focused on proteins in solution as templates for nanomaterial growth; for example, proteins have been used as cages for the synthesis of nanomaterials in solution[14–20]. Single crystals of proteins, on the other hand, are highly ordered three-dimensional structures with a large capacity to absorb water-based solutions. Thus, they can be regarded as porous materials[21–24]. Using a single protein crystal to template the *in situ* growth of gold nanoparticles slows down the fast kinetics of gold nanoparticle formation, and makes the system amenable for structural characterization and careful mechanistic studies.

Despite the promise of this approach, few studies have been devoted to the synthesis and characterization of nanomaterials within protein crystals, particularly in a time-dependent manner, because of several challenges[23,24]. First, growing single crystals of proteins is often difficult, and such single crystals, if grown successfully, contain delicate three-dimensional periodic structures and sophisticated interactions among the protein units, making it difficult to encapsulate nanomaterials within protein crystals by co-crystallization. Second, the necessary reagents (such as metallic precursors and strong reducing agents) and reactions (such as crosslinking of protein crystals and metallic salt reduction) often disrupt the crystalline lattice. Finally, there are no well-established methodologies with which to reveal the structural information for these bio-nano hybrids.

To explore the potential of protein-directed growth of nanomaterials in a single crystal, lysozyme was chosen for investigation, because it can be crystallized readily and is widely available in animals, plants, fungi, bacteriophages and bacteria[25,26]. Previously, Mann and co-workers have used crosslinked lysozyme single crystals to grow silver and gold nanostructures[24]. However, crosslinking has been shown to change the protein structure[24]. To provide deeper insights into the biomineralization of gold and the mechanism of biomolecule-directed gold nanoparticle formation, it is desirable to use native protein crystals. More importantly, it is essential to investigate the time-dependent, *in situ* growth of gold nanoparticles to obtain mechanistic insights. Gold nanoparticles within lysozyme single crystals were therefore synthesized from lysozyme and $ClAuS(CH_2CH_2OH)_2$ (referred to **Au(I)**) using an *in situ* approach. This approach significantly retards nanoparticle growth, allowing the reaction to be monitored in a time-dependent manner and also enabling the direct study of metal–protein interactions through X-ray crystallography. It also allows the gold nanoparticle structures to be monitored by transmission electron microscopy (TEM) and for their three-dimensional distribution to be analysed by electron tomography[27,28].

The crystals of lysozyme–**Au(I)** could be observed after one day of growth. Initially, the single crystals of lysozyme–**Au(I)** were colourless (Fig. 1a). The crystals gradually changed from colourless to pink, then to red as growth proceeded (Fig. 1a). We hypothesize that this colour evolution of the protein crystals originates from the characteristic surface plasmon resonance (SPR) absorption of nanostructured gold[1], thus indicating the growth of gold nanoparticles inside the protein crystals. The SPR absorption of the gold nanoparticles was also confirmed by an absorption spectrum, which demonstrated an absorption peak centred at 580 nm (Supplementary Fig. S1).

Gold nanoparticle growth within the protein crystals was confirmed by a time-dependent TEM study (Fig. 1b,c). At an early stage (for example, one day), no nanoparticles could be observed, consistent with the lack of colour in the crystal (Fig. 1a). From 1.5 days, gold nanoparticles were observed to form. Statistical analysis of the TEM images indicates that the gold nanoparticles grew gradually, beginning with a small average size of 2.9 nm after 1.5 days of growth, and increasing to 16.9 nm after 10 days (Fig. 1d). Interestingly, a bimodal size distribution was observed after 3 and 5 days, centring at 6.0 nm and 10.7 nm after 3 days of growth, and at 5.6 nm and 16.4 nm after 5 days of growth. The bimodal distribution became a single peak distribution after 10 days (Supplementary Fig. S3), with the growth rate being lower than in

[1]Department of Chemistry, University of Illinois at Urbana-Champaign, Urbana, Illinois 61801, USA, [2]Department of Materials Science and Engineering, University of Illinois at Urbana-Champaign, Urbana, Illinois 61801, USA, [3]George L. Clark X-Ray Facility and 3M Materials Laboratory, University of Illinois at Urbana-Champaign, Urbana, Illinois 61801, USA, [4]College of Bioengineering, Chongqing University, Sha Ping Ba Street 174, Chongqing, 400044, China, [5]Department of Biology, Brookhaven National Laboratory, Upton, New York 11973, USA. *e-mail: yi-lu@illinois.edu; jianzuo@illinois.edu; ianr@illinois.edu

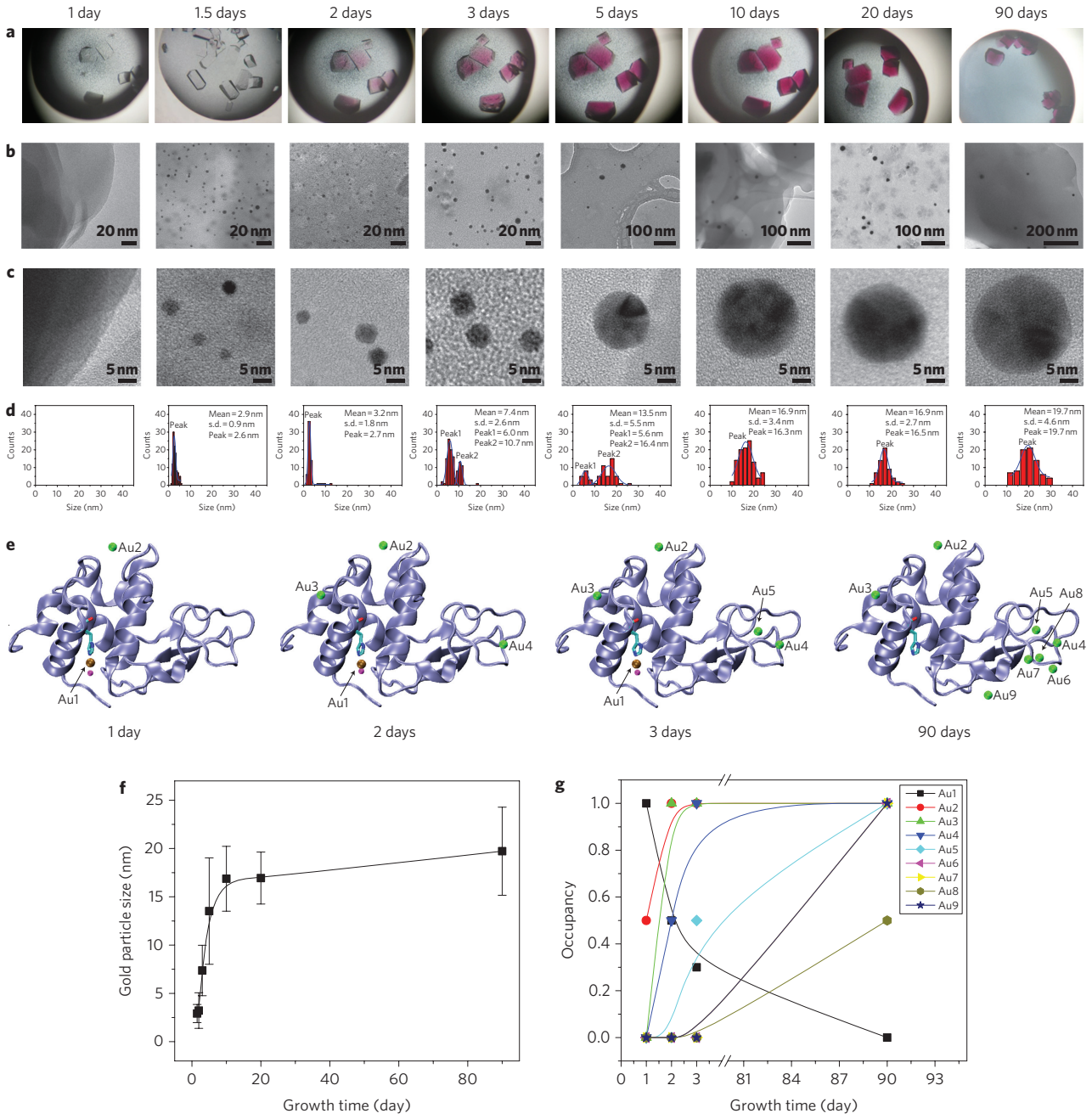

Figure 1 | Time-dependent, protein-directed growth of gold nanoparticles in single crystals. a, Optical images of single crystals of lysozyme grown in the presence of **Au(I)** at different days of growth. **b**–**d**, Corresponding TEM images at low magnification (**b**) and high magnification (**c**), and plots of the size distribution histograms (**d**) of the gold nanoparticles within the lysozyme crystals (s.d., standard deviation). **e**, X-ray crystal structures of the lysozymes from single crystals in **a** at the first, second, third and 90th days of growth. (**Au(I)**, ochre; **Au(III)**, green; carbon, cyan; nitrogen, blue; oxygen, red; chloride, magenta.) **f**, Time-dependent size evolution of gold nanoparticles based on their TEM images. **g**, Time-dependent occupancy evolution of different gold ions bound to the three-dimensional structure of lysozymes. The numbering scheme of gold ions is the same as in **e**.

the first 10 days. The time-dependent size evolution of gold nanoparticles is summarized in Fig. 1f.

Gold nanoparticle growth could originate from the spontaneous disproportionation of **Au(I)** to **Au(III)** and **Au(0)**, followed by accumulation of **Au(0)** into gold nanoparticles within the crystal. To confirm this hypothesis, **Au(I)** in aqueous solution without protein was incubated at room temperature, and a gold film formed within 4 h of incubation, suggesting that **Au(I)** disproportionated (Supplementary Fig. S4). These results suggest that the growth rate of the nanoparticles could be significantly lowered within a protein single crystal. This significant decrease in growth rate enabled us to carry out further studies on this time-dependent chemical reaction (**Au(I)** disproportionation and gold nanoparticle formation), as well as allowing us to assess the effects of the gold nanoparticles on the protein crystal structure. Additionally, to find out whether the nanoparticles within the protein crystals were formed due to co-crystallization of the lysozyme and preformed gold nanoparticles, we carried out control experiments using lysozyme solution and gold nanoparticles of different sizes under the same conditions as previously reported[29]. No encapsulation of gold nanoparticles within the protein crystals was observed for all three nanoparticles tested (Supplementary Fig. S5), suggesting

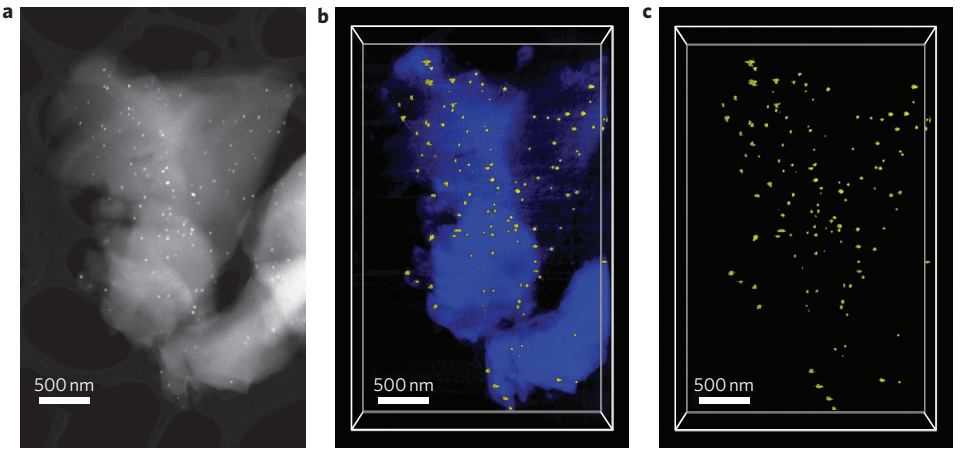

Figure 2 | HAADF-STEM images of the three-dimensional distribution of gold nanoparticles within lysozyme single crystals. a, HAADF-STEM image of gold nanoparticles within lysozyme single crystals at 0° tilt. **b**, Corresponding image of the three-dimensional tomographic reconstruction. **c**, As in **b**, but without lysozyme. In **a**, white dots indicate gold nanoparticles incorporated within the lysozyme matrix, which is slightly darker. In **b** and **c**, gold nanoparticles are in yellow and lysozyme crystals are in blue.

that *in situ* growth was critical to encapsulating nanoparticles within lysozyme single crystals. This growth process provided a unique approach to preparing nanoparticle-in-crystal hybrids (Supplementary Fig. S6).

Inside the protein crystal, the gold nanoparticles evolved from small single nanocrystals to larger multiple twinned particles (Supplementary Figs S7 and S8). The crystalline nature of the nanoparticles grown in the lysozyme crystals was further confirmed by powder X-ray diffraction. Material supporting these observations, including high-resolution TEM images of the nanoparticles at different growth stages and the powder XRD pattern, are shown in Supplementary Figs S7, S8 and S9.

To further confirm the entrapment of gold nanoparticles within protein crystals and to visualize their distribution, we performed electron tomography, a technique used successfully in previous studies[28,30]. High-angle annular dark-field scanning transmission electron microscopy (HAADF-STEM) was used to collect a series of images at different tilt angles for tomographic reconstruction through its effective suppression of coherent diffraction and Z-contrast imaging[28,31]. Because the gold nanoparticles and the lysozyme crystal matrix have a large Z difference, the contrast is sufficient for tomographic reconstruction. Figure 2a shows a HAADF-STEM image of gold nanoparticles within the lysozyme single crystals at 0° tilt. Figure 2b,c shows the corresponding tomograms of this tilt series. The nanoparticles in Fig. 2a can be laid over those in Fig. 2b,c well, suggesting a successful reconstruction. From a combination of the tomograms in Fig. 2b,c (and their corresponding movies in the Supplementary Information), it is clear that the nanoparticles were three-dimensionally incorporated into the lysozyme crystals with a relatively even distribution; this result further confirms that their growth occurred within the lysozyme single crystals.

Despite the incorporation of hundreds of gold nanoparticles and the fact that no crosslinking method was used, the lysozyme crystals remained intact throughout this growth process (Supplementary Fig. S6)[24]. As shown in Fig. 1a, the lysozyme crystals housing gold nanoparticles maintained their single-crystal structure, indicating that the *in situ* growth method did not disrupt the crystal structures. This feature allowed us to study the binding sites for gold atoms in the protein and to elucidate the mechanism of formation of the nanoparticles by using high-resolution X-ray crystallography. As shown in Fig. 1e, we successfully obtained time-dependent, high-resolution X-ray crystallographic structures of the crystals grown from lysozyme and **Au(I)**, at different growth stages. From these structures, **Au(I)** binding sites, its subsequent disproportionation and further reactions (the formation of gold nanoparticles and their rebinding to lysozyme as **Au(III)**) could be elucidated.

As shown in Fig. 1e, two gold atoms were observed in the crystal structure on the first day. One atom, named Au1, was coordinated by the ε-N of His15 and a chloride atom in a linear geometry. The other gold atom, Au2, interacted with Tyr23 (see Supplementary Fig. S10 for a detailed binding motif). As the crystal growth proceeded, an increasing number of gold atoms were observed to bind to the protein. Two additional gold atoms, Au3 and Au4, were found on the second day, and a fifth one, Au5, was found on the third day (Fig. 1e). Interesting results were observed on the 90th day, as four more gold atoms (Au6, Au7, Au8, Au9) were found, and the Au1 bound to His15 disappeared (Fig. 1e).

As the Au1 was in a linear geometry (ε-N-Au-Cl) with an angle of 176.38°, characteristic of +1 valence gold complexes (Supplementary Fig. S10)[32], we assigned Au1 to the +1 valence state. However, the coordination geometries of the other gold atoms were not well-defined in the X-ray crystal structures due to a lack of coordinating ligands from the protein crystals, and it was difficult to assign their valence state from the structure alone. A crystal was therefore grown from the lysozyme and **Au(III)** (as $HAuCl_4$). As shown in Supplementary Fig. S11a, seven gold atoms, Au2′ to Au8′, were observed in the crystal of lysozyme–$HAuCl_4$. Because they overlaid the Au2 to Au8 atoms in the crystals of lysozyme–**Au(I)** very well (Supplementary Fig. S11b), we assigned Au2 to Au9 to the +3 valence state.

By combining the X-ray crystallography results and the electron microscopy observations, we propose the following mechanism to explain the chemical reactions and nanoparticle growth within the single crystal (Fig. 3). During protein crystal growth using lysozyme and **Au(I)**, **Au(I)** initially binds specifically to the ε-N of the His15 of the lysozyme. As the reaction proceeds, the **Au(I)** dissociates from His15 and disproportionates into **Au(0)** and **Au(III)** within the crystals. Meanwhile, free **Au(I)** in the mother liquor diffuses continuously into the lysozyme crystals and then also disproportionates into **Au(0)** and **Au(III)** within the crystals. Inside the crystals, **Au(0)** is further assembled into gold nanoparticles as large as 20 nm, and **Au(III)** translocates and rebinds to the other sites in the lysozyme (for example, Au2 to Au9), as shown in the crystallographic structures (Figs 1e, 3; Supplementary Fig. S13). A least-squares refinement of the crystallographic structures indicated that as the reaction proceeds, the occupancy of Au1 decreases from 1 to 0, whereas that of the other gold atoms gradually increases (Fig. 1g). For Au2, Au3, Au4, Au5, Au6, Au7 and Au9, the

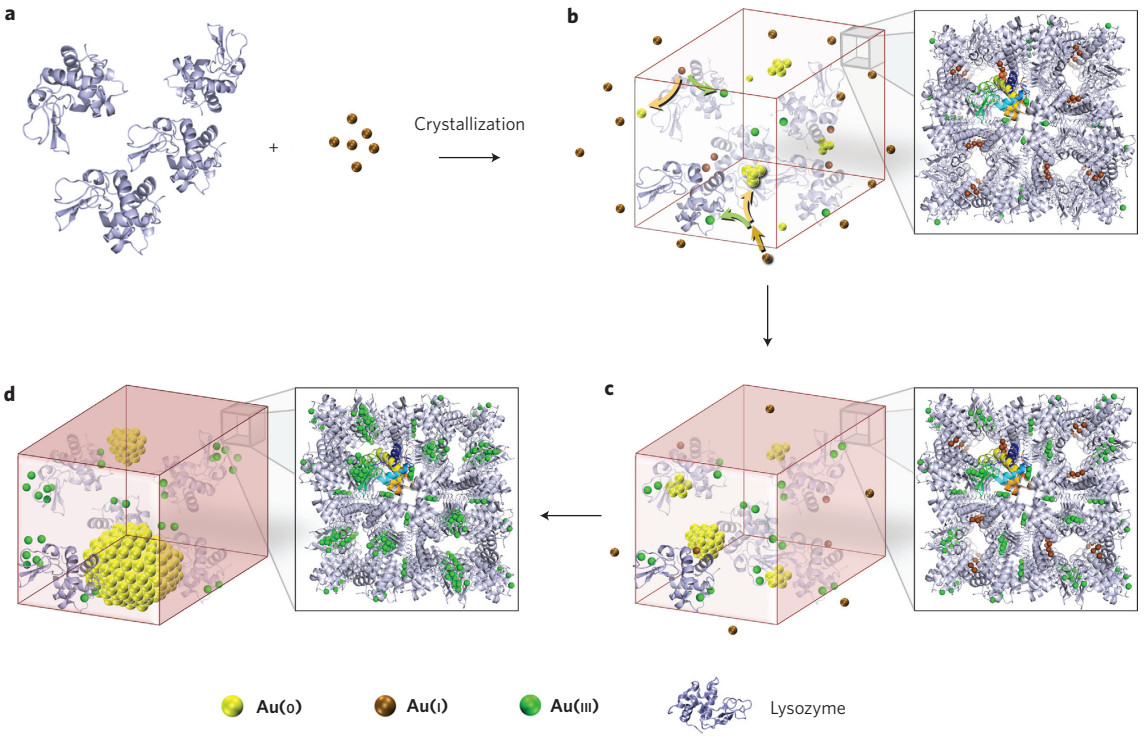

Figure 3 | Schematic of gold nanoparticle growth within a lysozyme single crystal. a, Lysozyme (blue) and **Au(I)** (ochre) are mixed to allow the protein crystals to grow. **b**, **Au(I)** is initially bound specifically to the ϵ-N of His15 of the lysozyme, and then dissociates from His15 and disproportionates into **Au(0)** (yellow) and **Au(III)** (green). Meanwhile, **Au(I)** in the mother liquor diffuses continuously into the lysozyme crystals and then disproportionates into **Au(0)** and **Au(III)**. **Au(0)** then grows into small gold clusters (the gold clusters are too small to render the crystal red at this early stage) and the **Au(III)** translocates and rebinds the lysozyme. **c**, As the process proceeds, more **Au(I)** disproportionates into **Au(0)**, making the small gold clusters grow larger, into nanoparticles, rendering the crystal red due to their characteristic SPR absorption. At the same time, more **Au(III)** are generated from the disproportionation and translocate and rebind the lysozyme. **d**, Finally, **Au(I)** disappears and a large number of ~20 nm gold nanoparticles form within the crystal, while eight **Au(III)** rebind to the lysozyme. The enlarged pictures in **b**–**d** show experimentally determined crystallographic packing of lysozyme proteins with gold ions inside. For clarity of the scheme, the lysozyme proteins are not drawn to scale in the three-dimensional protein crystals.

occupancies increase to 1 after 90 days of growth; for Au8, the occupancy increases to 0.5 after 90 days. In addition, the size evolution of the gold nanoparticles within the crystals was well correlated with the occupancy changes of the gold atoms, with a decrease in the occupancy of Au1 being concomitant with the increase in the occupancies of Au2 to Au9 and the increase in size of the nanoparticles (Fig. 1f,g). These results further confirm the proposed reaction mechanism (Fig. 3; Supplementary Fig. S13).

Having achieved the *in situ* growth of gold nanoparticles within a the increase in lysozyme single crystal and gaining an understanding of the mechanism, we also wished to fine-tune the growth of the nanoparticles. As shown in Fig. 1 and Supplementary Fig. S14, the size of the gold nanoparticles could be tuned by controlling the growth time. In addition, many other species (such as the metal ions and small molecule ligands that are present in the gold biomineralization reaction, in the biogenic formation of gold nanoparticles and in biomedical applications using these bionanomaterials) may influence the rate of nanoparticle growth, so we investigated their effects on nanoparticle growth within the crystal. Interestingly, we found that Hg^{2+} could significantly accelerate nanoparticle growth rate (and thus nanoparticle size), and *tris*(2-carboxyethyl)phosphine (TCEP) could decelerate nanoparticle growth rate (and thus nanoparticle size) (Supplementary Figs S16,S17). Moreover, the growth rate could be fine-tuned by changing the concentration of the additives. The acceleration of gold nanoparticle growth by Hg^{2+} could originate from specific interactions between Hg^{2+} and Au^{+} ions[33], while the deceleration induced by TCEP could be due to a stronger interaction between gold and TCEP than between gold and $S(CH_2CH_2OH)_2$ (Supplementary Figs S18,S19)[32,34]. These results suggest that it is possible to further control particle growth within a crystal by using external chemical stimuli.

In summary, we have demonstrated time-dependent, *in situ* growth of gold nanoparticles within single crystals of lysozyme, without disturbing the protein crystalline lattice or the three-dimensional protein structure. The growth of the gold nanoparticles, their three-dimensional distribution, and the interaction of gold atoms with the lysozyme were revealed by TEM, as well as tomography and X-ray crystallography. The results show that proteins can direct gold nanoparticle formation through specific interactions with histidine residues, and the presence of other chemicals such as metal ions or metal-binding ligands can play important roles in fine-tuning the growth process. Preliminary investigations have shown that other proteins, such as thaumatin from *Thaumatococcus daniellii*, could also be used as the host matrix for *in situ* growth of gold nanoparticles within protein single crystals (Supplementary Fig. S20), suggesting that this method can be general. This work could provide a new approach to studying the interactions between biomolecules and nanomaterials, and the mechanism of biomineralization[6,7,13,35]. Furthermore, it could allow novel nanomaterial-in-protein crystal hybrids to be synthesized with applications in catalysis, optical and plasmonic devices, and sensing[23,24].

Received 4 October 2010; accepted 13 December 2010; published online 30 January 2011

References

1. Daniel, M. C. & Astruc, D. Gold nanoparticles: assembly, supramolecular chemistry, quantum-size-related properties, and applications toward biology, catalysis, and nanotechnology. *Chem. Rev.* **104,** 293–346 (2004).
2. Rosi, N. L. & Mirkin, C. A. Nanostructures in biodiagnostics. *Chem. Rev.* **105,** 1547–1562 (2005).
3. De, M. *et al.* Sensing of proteins in human serum using conjugates of nanoparticles and green fluorescent protein. *Nature Chem.* **1,** 461–465 (2009).
4. Murphy, C. J. *et al.* Gold nanoparticles in biology: beyond toxicity to cellular imaging. *Acc. Chem. Res.* **41,** 1721–1730 (2008).
5. Xie, J. P., Zheng, Y. G. & Ying, J. Y. Protein-directed synthesis of highly fluorescent gold nanoclusters. *J. Am. Chem. Soc.* **131,** 888–889 (2009).
6. Reith, F., Rogers, S. L., McPhail, D. C. & Webb, D. Biomineralization of gold: biofilms on bacterioform gold. *Science* **313,** 233–236 (2006).
7. Reith, F. *et al.* Mechanisms of gold biomineralization in the bacterium *Cupriavidus metallidurans*. *Proc. Natl Acad. Sci. USA* **106,** 17757–17762 (2009).
8. Lengke, M. F. & Southam, G. The effect of thiosulfate-oxidizing bacteria on the stability of the gold–thiosulfate complex. *Geochim. Cosmochim. Acta* **69,** 3759–3772 (2005).
9. Karthikeyan, S. & Beveridge, T. J. *Pseudomonas aeruginosa* biofilms react with and precipitate toxic soluble gold. *Environ. Microbiol.* **4,** 667–675 (2002).
10. Kashefi, K., Tor, J. M., Nevin, K. P. & Lovley, D. R. Reductive precipitation of gold by dissimilatory Fe(III)-reducing bacteria and archaea. *Appl. Environ. Microbiol.* **67,** 3275–3279 (2001).
11. Karamushka, V. I., Ulberg, Z. R. & Gruzina, T. G. The role of membrane processes in bacterial accumulation of Au(III) and Au(0). *Ukr. Biokhimicheskii Zhurnal* **62,** 76–82 (1990).
12. Carney, C. K., Harry, S. R., Sewell, S. L. & Wright, D. W. Detoxification biominerals. *Top. Curr. Chem.* **270,** 155–185 (2007).
13. Mann, S. (eds) *Biomineralization: Principles and Concepts in Bioinorganic Materials Chemistry* (Oxford Univ. Press, 2001).
14. Meldrum, F. C., Wade, V. J., Nimmo, D. L., Heywood, B. R. & Mann, S. Synthesis of inorganic nanophase materials in supramolecular protein cages. *Nature* **349,** 684–687 (1991).
15. Uchida, M. *et al.* Biological containers: protein cages as multifunctional nanoplatforms. *Adv. Mater.* **19,** 1025–1042 (2007).
16. Medalsy, I. *et al.* SP1 protein-based nanostructures and arrays. *Nano Lett.* **8,** 473–477 (2008).
17. Butts, C. A. *et al.* Directing noble metal ion chemistry within a designed ferritin protein. *Biochemistry* **47,** 12729–12739 (2008).
18. Ueno, T. *et al.* Process of accumulation of metal ions on the interior surface of apo-ferritin: crystal structures of a series of apo-ferritins containing variable quantities of Pd(II) Ions. *J. Am. Chem. Soc.* **131,** 5094–5100 (2009).
19. Ueno, T., Abe, S., Yokoi, N. & Watanabe, Y. Coordination design of artificial metalloproteins utilizing protein vacant space. *Coord. Chem. Rev.* **251,** 2717–2731 (2007).
20. Dickerson, M. B., Sandhage, K. H. & Naik, R. R. Protein- and peptide-directed syntheses of inorganic materials. *Chem. Rev.* **108,** 4935–4978 (2008).
21. Margolin, A. L. & Navia, M. A. Protein crystals as novel catalytic materials. *Angew. Chem. Int. Ed.* **40,** 2205–2222 (2001).
22. Koshiyama, T. *et al.* Modification of porous protein crystals in development of biohybrid materials. *Bioconjugate Chem.* **21,** 264–269 (2010).
23. Falkner, J. C. *et al.* Virus crystals as nanocomposite scaffolds. *J. Am. Chem. Soc.* **127,** 5274–5275 (2005).
24. Guli, M., Lambert, E. M., Li, M. & Mann, S. Template-directed synthesis of nanoplasmonic arrays by intracrystalline metalization of cross-linked lysozyme crystals. *Angew. Chem. Int. Ed.* **49,** 520–523 (2010).
25. Jolles, P. & Jolles, J. Whats new in lysozyme research—always a model system, today as yesterday. *Mol. Cell. Biochem.* **63,** 165–189 (1984).
26. Sanders, L. K. *et al.* Control of electrostatic interactions between F-actin and genetically modified lysozyme in aqueous media. *Proc. Natl Acad. Sci. USA* **104,** 15994–15999 (2007).
27. Kawamichi, T., Haneda, T., Kawano, M. & Fujita, M. X-ray observation of a transient hemiaminal trapped in a porous network. *Nature* **461,** 633–635 (2009).
28. Li, H. Y., Xin, H. L., Muller, D. A. & Estroff, L. A. Visualizing the 3D internal structure of calcite single crystals grown in agarose hydrogels. *Science* **326,** 1244–1247 (2009).
29. Hodzhaoglu, F., Kurniawan, F., Mirsky, V. & Nanev, C. Gold nanoparticles induce protein crystallization. *Cryst. Res. Technol.* **43,** 588–593 (2008).
30. Arslan, I., Yates, T. J. V., Browning, N. D. & Midgley, P. A. Embedded nanostructures revealed in three dimensions. *Science* **309,** 2195–2198 (2005).
31. Browning, N. D., Chisholm, M. F. & Pennycook, S. J. Atomic-resolution chemical analysis using a scanning transmission electron microscope. *Nature* **366,** 143–146 (1993).
32. Puddephatt, R. J. (eds) *The Chemistry of Gold (Topics in Inorganic and General Chemistry, Monograph 16)* (Elsevier Scientific Publishing, 1978).
33. Pyykko, P. Theoretical chemistry of gold. *Angew. Chem. Int. Ed.* **43,** 4412–4456 (2004).
34. Ralle, M., Lutsenko, S. & Blackburn, N. J. X-ray absorption spectroscopy of the copper chaperone HAH1 reveals a linear two-coordinate Cu(I) center capable of adduct formation with exogenous thiols and phosphines. *J. Biol. Chem.* **278,** 23163–23170 (2003).
35. Lichtenegger, H. C., Schoberl, T., Bartl, M. H., Waite, H. & Stucky, G. D. High abrasion resistance with sparse mineralization: copper biomineral in worm jaws. *Science* **298,** 389–392 (2002).

Acknowledgements

This work was supported by the US National Science Foundation (CMMI 0749028 and DMR-0117792). The authors thank C. Lei and J. Wen for help with the (S)TEM imaging, L.A. Miller for the preparation of microtome samples and 75 kV TEM imaging, J. Soares for solid-state absorption spectroscopic measurements, M. Sardela for XRD measurements, and Y.-W. Lin, N.M. Marshall, S.-L. Tian, H.E. Ihms and K.-D. Miner for helpful discussions. J.Z. and J.M.Z. are supported by DOE DEFG02-01ER45923. S.H. and I.M.R. acknowledge support from the US Department of Energy (grant DE-FC36-05GO15064). (S)TEM experiments were carried out in part in the Frederick Seitz Materials Research Laboratory Central Facilities, University of Illinois.

Author contributions

H.W., Z.W. and Y.L. designed the research. H.W., Z.W., J.Z., Y.-G.G., L.Y. and H.R. performed the research. H.W., Z.W., J.Z., S.H., Y.-G.G., L.Y., H.R., L.H.T., H.X., C.H., I.M.R., J.-M.Z. and Y.L. analysed the data. All authors co-wrote the paper.

Additional information

The authors declare no competing financial interests. Crystallographic data have been deposited in the Protein Data Bank under accession codes 3P4Z, 3P64, 3P65, 3P66 and 3P68. Supplementary information accompanies this paper at www.nature.com/naturenanotechnology. Reprints and permission information is available online at http://npg.nature.com/reprintsandpermissions/. Correspondence and requests for materials should be addressed to Y.L., J.M.Z. and I.M.R.